Experimental Investigation on the Behavior of Artificial Magnetic Cilia

Andrea MARUCCI, Giovanni P. ROMANO*

* Corresponding author: Tel.: ++39 0644585913; Fax: ++39 0644585250;
Email: giampaolo.romano@uniroma1.it
Dept. Mechanical & Aerospace Engineering, University of Roma "La Sapienza", Rome, ITALY

Abstract. In the present work, the flow fields induced by the movement of artificial cilia under the effect of a magnetic field are investigated. In order to obtain almost steady conditions, the set-up consists of fixed cilia which oscillate under the action of a rotating magnetic field. The aim of the work is to determine under which geometrical configurations a net flow rate or a global mixing is obtained. The results show that cilia mounted in the direction of rotation allow net fluid flow, whereas those in radial position have larger turbulent kinetic energy. Thus, the former could be used as micro-pump, whereas the latter as micro-mixer.

Keywords: Micro Flow, Magnetic Cilia, Micro-Mixer, Micro-Pump

1. Introduction

The use of micro-devices is nowadays widely increasing due to the huge amount of applications in medical devices, biomedicine, micro-sensors and control, micro-mixers and pumps (Santiago *et al.* 1998, Laser and Santiago 2004, Kallio and Kuncova 2004, Squires and Quake, 2005, Lindken *et al.* 2009). Specifically, it is challenging to design systems at micro-scales which could ensure net flow rates or mixing without any direct contact of the fluid with external parts to avoid contamination, especially when dealing with drugs and medical devices. To this end, the use of magnetically actuated cilia received recently a large attention (Hussong *et al.* 2011a, Khaderi *et al.* 2011). Indeed, starting from observations made in nature, under the hypothesis of metachronal movement, an ensemble of cilia ensures that a net flow rate is possible (Purcell 1977, Vogel 1996, Hussong *et al.* 2011b). Therefore, it is important to verify under which conditions, such as type of forcing, cilia geometry and material, an overall flow displacement is possible and what is its effective amount (Niedermayer, 2008). On the other hand, even if a net flow rate is not achieved, it is still possible that cilia ensured an effective mixing of the flow, thus allowing a useful interaction between the fluid and the injected scalar solution. Starting from this point, the aim of the present experimental investigation is to verify in a scale up model under which geometrical configuration, the array of cilia is able to give a net flow rate or a global mixing. In order to obtain an arrangement in almost steady conditions, the cilia are mounted on a disk placed over a rotating magnetic field.

2. Device set-up and specifications

The rotating disk with the magnetic element is placed under a circular plate containing the cilia, which are themselves coated by a magnetic paint. The angular velocity of the magnetic element is 0.5 round/s. The cilia have a length of about 10 mm and a diameter of 1 mm and are placed in an annulus achieved on a circular plate, with rectangular cross section of 40 mm^2. The Reynolds number, based on the cilia length and maximum observed velocity (5 mm/s) is around 50, so clearly within the laminar regime as expected for real cilia. They are mounted radially and under the action of the rotating magnetic field display an oscillating behavior by moving in the direction of rotation and then turning back into the initial position.

Images of the whole rotating disk with the three cilia geometries are presented in Figure 1. The attention is here focused onto the geometrical configuration of the cilia and specifically on the inclination angle in respect of the rotating magnetic field (clockwise), as also defined in Figure 1.

Three values have been tested, *i.e.* 30° inclined in the direction of rotation, 90° (called also radial position) and 150° in the direction counter rotation. The two components of velocity measured on the plane are the tangential (*i.e.* along the direction of rotation) and the radial ones. The cilia spacing is about one half of their length, *i.e.* about 5 mm. The size of the imaged region is around 10 mm × 13 mm (corresponding to 2 to 3 cilia), as indicated by the red dotted boxes in Figure 1. About 1000 images of such a region are acquired through a high-speed camera with a spatial resolution of 1024 pixel × 768 pixel at a frame rate of 30 Hz (AVT-Pike). The camera was set with a shutter time equal 1/150 s and equipped with a 50 mm F1.4 Nikon objective in addition to a macro extension of 12 mm. The magnification factor is about 50 pixel/mm and a high power lamp is used for illumination (400 W). A second series of images with a larger portion of the flow field was also acquired by means of a 28 mm Nikon objective.

Examples of acquired images from the two series are presented in Figure 2, where the flow tracers are clearly visible with some particle clustering, while the cilia appear only as dark shadows. From this point of view, it is important to consider that the measurement plane (*i.e.* the one at which the camera objective is focused) is slightly above the cilia so that the flow is moving over them. As seeding particles, hollow glass styrene spheres with mean diameter equal to 10 µm have been used, with density equal to 1.06 times that of flow. Thus, these tracers feel very low buoyancy forces and are insensitive to the magnetic field. Two consecutive frames are analyzed, in order to determine the flow tracer displacements during the alternating motion of the cilia, using Particle Image Velocimetry (PIV) technique.

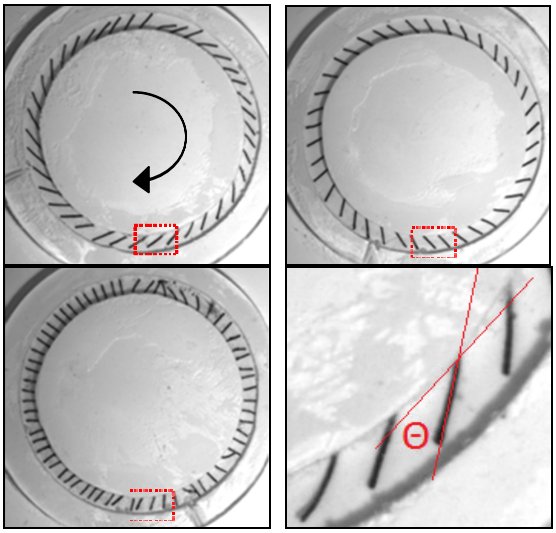

Figure 1. The three tested cilia geometries: inclined with the flow (at the top left), counter flow (at the top right) and placed radially (at the bottom left). Definition of the inclination angle is added at the bottom right.

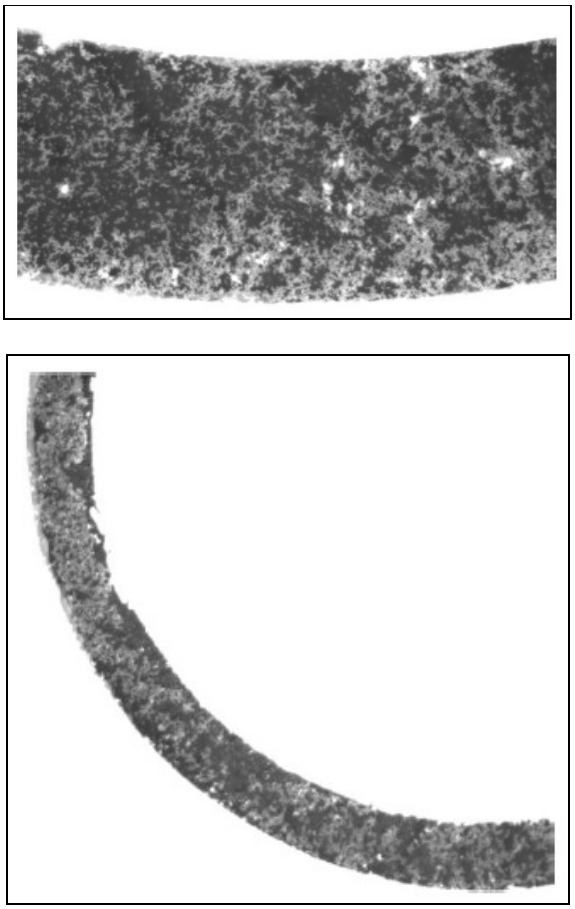

Figure 2. Examples of acquired images with seeding particles. The investigated region containing 2-3 cilia as in the rectangular box of Figure 1 (at the top) and one quarter annulus general view (at the bottom).

After low-pass sharpen filtering of the images, an advanced cross-correlation commercial PIV algorithm with window offset and deformation is employed (DaVis by LAVISION GmbH). Specifically, an iterative processing starting from interrogation windows of 64×64 pixel with overlapping equal to 75% down to 32×32 pixel windows with the same overlapping is adopted. Image post-processing based on moving average validation and iterative replacement has been also employed. Statistical moments of the two velocity components on the measurement plane, are computed on the basis of 500 image couples. This means that the maximum statistical error on the mean value is around 3% (this is also the order of magnitude of the error on the flow rate), while on *rms* values this raises up to 5%.

3. Results and Discussion

In Figure 3, the time average vector field is shown for the cilia inclined by 30° in the direction of rotation (the reference vector on the left upper corner is equal to 5 pixel/frame = 3 mm/s). A net flow from right to left, *i.e.* in the direction of the rotating magnet, can be observed, more concentrated at the top (at the root of the cilia) than at the bottom where the velocity is approaching zero. The overlapping with cilia at rest position indicates that the fluid motion is not continuous, but mainly located in the front part of the cilia roots. Thus, it seems that this rigid portion is the one mainly acting as fluid driving element, whereas at the cilia apex the forward and backward motions result in a zero net flux. This is confirmed from the data presented in Figure 4, where the color maps of average tangential and radial velocities are reported. From the first figure, a net positive flow from right to left with maximum tangential velocities equal approximately to 4 mm/s is observed. This has to be compared with the tangential velocity of the rotating magnet which is approximately 30 mm/s. By computing the bulk velocity in the measurement section, using the cross-sectional area, it is possible to evaluate the net flow rate which is approximately 60 mm^3/s.

On the other hand, the radial velocity alternates between positive and negative values not larger than 1 mm/s, originated from the cilia oscillatory motion, which gives a wavy mean flow pattern also observed in Figure 3.

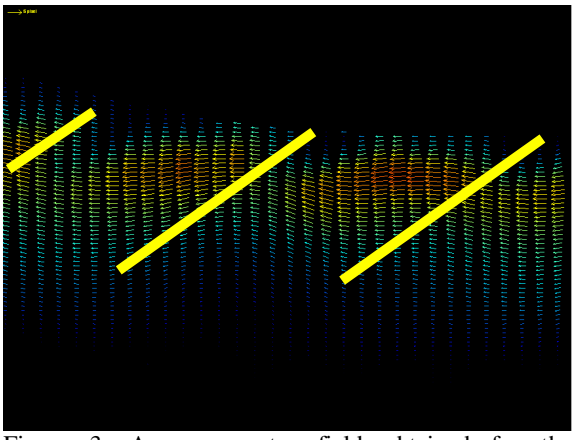

Figure 3. Average vector field obtained for the configuration with cilia inclined by 30° in the direction of rotation. The color indicates the vector magnitude. The cilia positions at rest are also shown.

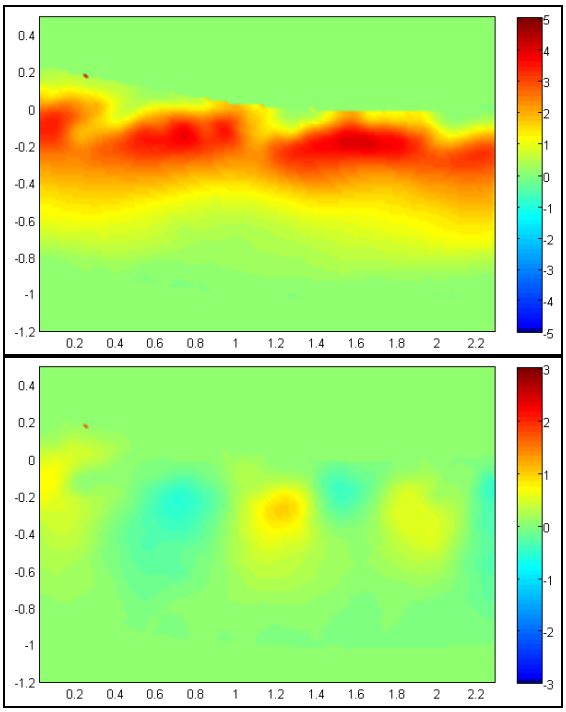

Figure 4. Color maps of average tangential (at the top) and radial (at the bottom) velocities for cilia inclined by 30° in the direction of rotation. The axis are made non-dimensional by the cavity radius (1 cm), whereas the colorbar is in mm/s.

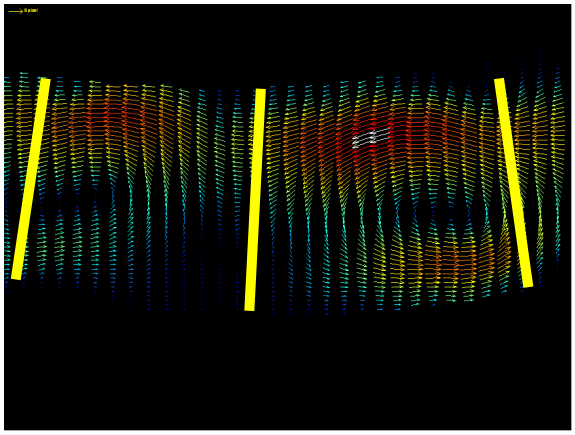

Figure 5. Average vector field obtained for the configuration with cilia in radial position. The color indicates the vector magnitude. The cilia positions at rest are also shown.

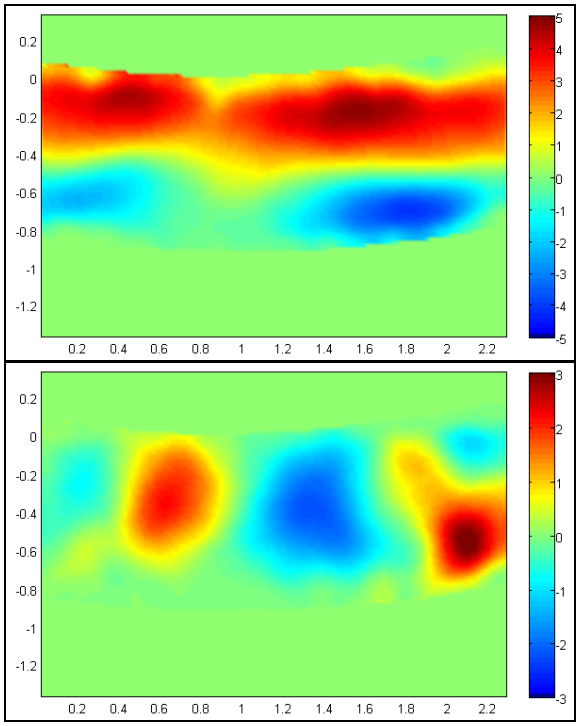

Figure 6. Color maps of average tangential (at the top) and radial (at the bottom) velocities for the cilia in radial position. The axis are made non-dimensional by the cavity radius (1 cm), whereas the colorbar is in mm/s.

In the condition of cilia positioned radially (at 90° in comparison to the tangential direction), the situation changes. The average vector field for this conditions is presented in Figure 5. While the upper part of the mean flow is almost similar to the previous case, with even larger velocities, there is a clear backward flow at the cilia apex.

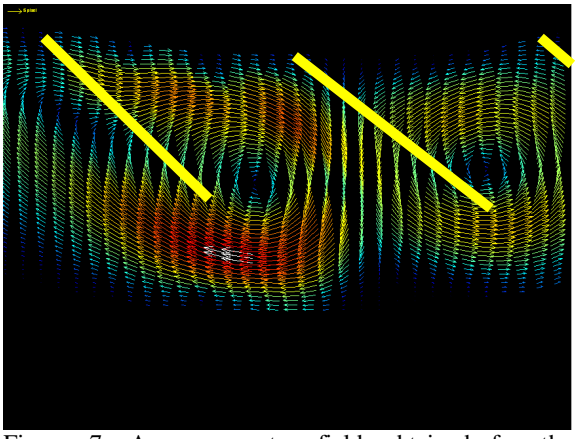

Figure 7. Average vector field obtained for the configuration with cilia inclined counter rotation. The color indicates the vector magnitude. The cilia positions at rest are also shown.

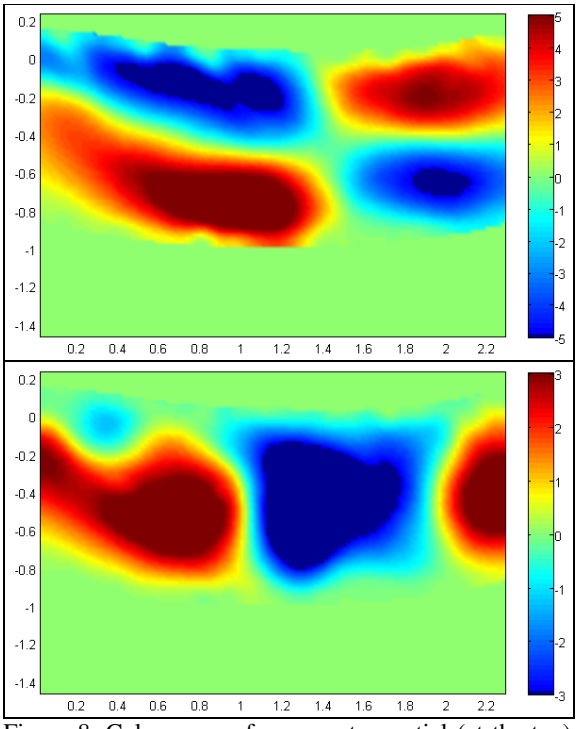

Figure 8. Color maps of average tangential (at the top) and radial (at the bottom) velocities for the cilia inclined counter rotation. The axis are made non-dimensional by the cavity radius (1 cm), and the colorbar is in mm/s.

The cilia position at rest, clearly indicates that this flow depends on the reversing motion of the cilia back to the initial position after finishing the moving magnet action. Nonetheless, there is still a net flux in the direction of the rotating magnet as displayed by the single velocity component color maps shown in Figure 6. Indeed, the counter

clockwise motion at the cilia root, with maximum tangential velocity around 5 mm/s is not completely balanced by the clockwise motion at the cilia apex, with a maximum negative velocity approximately equal to -4 mm/s.Therefore, the net flow rate is around 60% of the previous case, *i.e.* about 35 mm^3/s.The radial velocities are now much larger than in the previous case with a maximum absolute value equal to 3 mm/s.

The third investigated condition is that with the cilia mounted counter the rotation of the magnet (the angle is opposite to that of the first configuration). As shown in Figure 7, only alternate vortices are generated by cilia oscillations.Thus, in comparison with the other configurations, there is not a forward net fluid motion, rather resulting both forward and backward motions.The color maps of the tangential and radial velocity components, presented in Figure 8, confirm this behavior, which produces maximum tangential absolute velocities much larger than before (approximately 7 mm/s) and also higher radial velocity (around 5 mm/s). The fact that the mean field is rather well defined, indicates that the observed vortices are also stable in their positions and intensities.

Instantaneous fields allow understanding the specific mechanism which generates a net fluid motion.

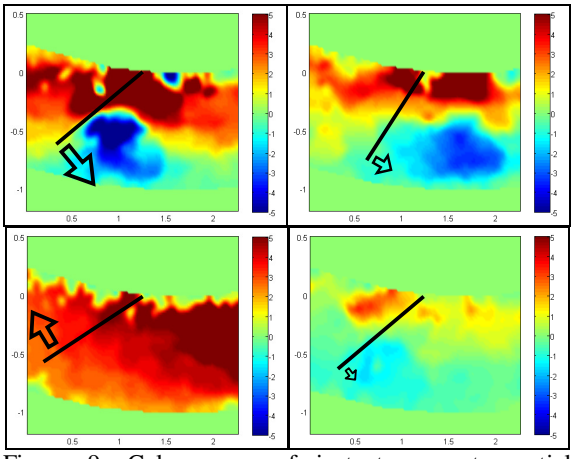

Figure 9. Color maps of instantaneous tangential velocity for cilia inclined by 30° in the direction of rotation during the passage of the magnet (actual position and velocity of one cilium is overlapped). Axis and colorbar are reported as in previous figures.

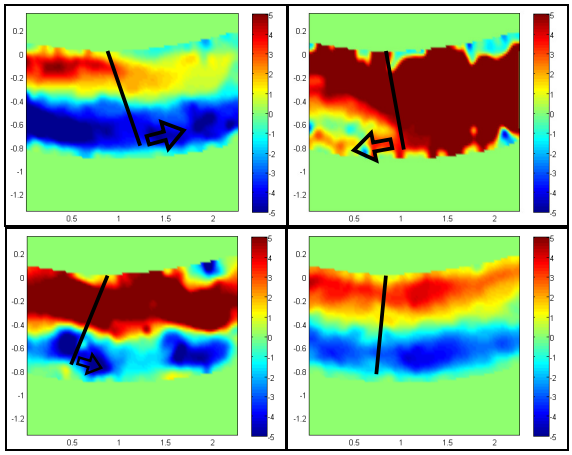

Figure 10. Color maps of instantaneous tangential velocity for cilia in radial position during the passage of the magnet (actual position and velocity of one cilium is overlapped). Axis and colorbar are reported as in previous figures.

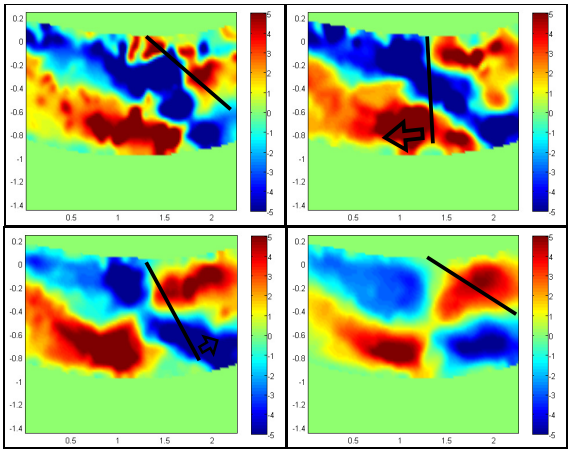

Figure 11. Color maps of instantaneous tangential velocity for cilia inclined counter rotation during the passage of the magnet (actual position and velocity of one cilium is overlapped). Axis and colorbar are reported as in previous figures.

In instantaneous plots, the oscillating behavior of the cilia is overlapped to velocity fields. Thus, instantaneous color plots of the tangential velocity are shown in Figure 9 for the configuration with cilia inclined by 30°. It is noticed that as the magnet is passing through the imaged region, the cilia are deflected towards the incoming magnet, thus generating a counter rotation flow (plots on the upper row). When the magnet passes through the region, a strong fluid motion in the direction of rotation is forced by the cilia (left plot at the bottom), whereas the cilia returns slowly to the

rest position after the magnet passage (right plot at the bottom). These plots allow understanding that the mean motion is generated mostly at the cilia root (even if there the cilia movement is small), because at the apex the net flow is low due to the cilia backward and upward oscillations.

Similar information can be derived from the other two configurations. From instantaneous plots of the cilia in radial position presented in Figure 10, it is possible to point out the backflow before the magnet passage and the following fluid motion (in the first row) and the quite strong backward flow when cilia are coming back to the initial position. This specific phenomenon is rather different from what observed in the 30° configuration. It gives rise to the higher counter-flow observed in the average plot of Figure 6. The situation for the third configuration is reported in Figure 11. In this case, the two counter-rotating vortices are always well established, except for the moment just before and after the magnet passage (first row in the figure). In comparison to the previous geometrical configurations of the cilia, this is the condition without any instant with strong global net flow motion in the direction of the rotating magnet, as confirmed by the average plot of Figure 8.

Another important question to be raised is if the movement of the cilia generates a global fluid motion in the whole apparatus or only at specific angular positions (as for example the one selected for the measurements). Therefore, a specific test has been performed on a much larger region, including a significant portion of the ring. The results are presented in Figure 12 for the three cilia configurations. It is possible to point out that for the cilia inclined in the direction of rotation a net fluid motion is present all over the apparatus except for a few backflow regions in the external part. This is in agreement with previous findings derived from measurements on the small region, which indicate that the major portion of the motion was located at the cilia root.

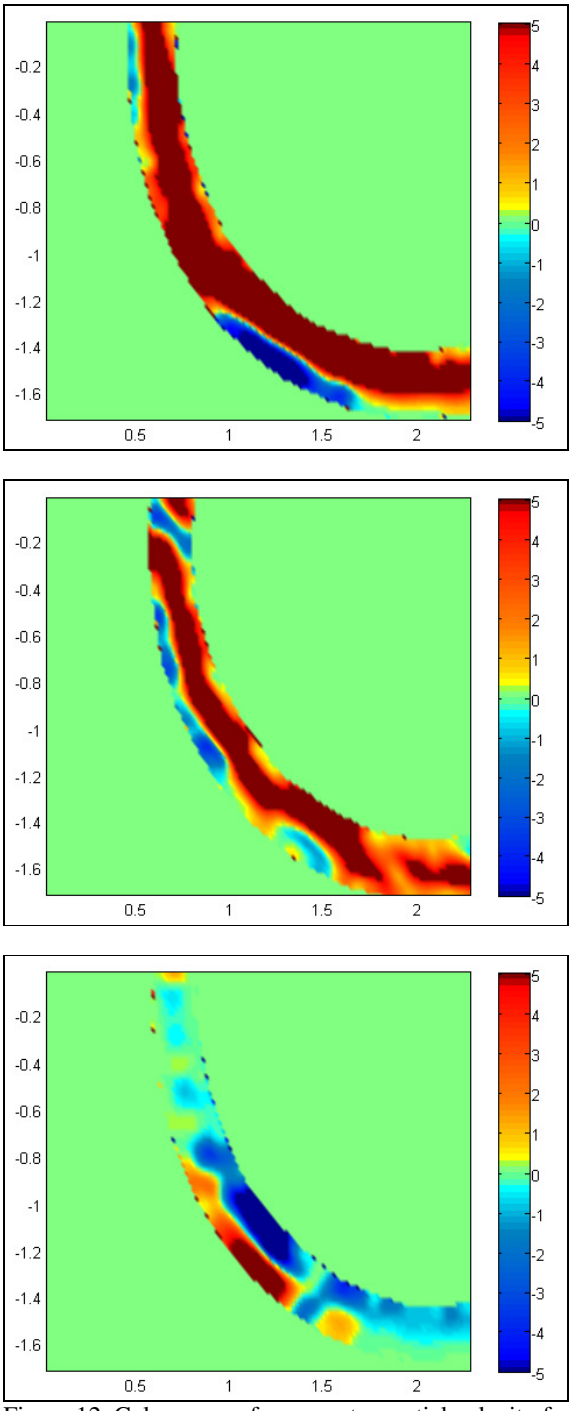

Figure 12. Color maps of average tangential velocity for the cilia inclined in the direction of rotation (at the top), in radial position (at the middle) and counter rotation (at the bottom). The axis are made non-dimensional by the cavity radius (1 cm), whereas the colobar is in mm/s.

For the cilia mounted in radial position, the number of those backflow regions is increasing, thus confirming a strong reverse flow at cilia apex. The number of alternating positive and negative flows is even larger and their extension is decreasing for the configuration with cilia mounted counter rotation, without a relevant net fluid motion. In all geometrical configurations, the results attained in a larger portion of the apparatus confirm the results obtained in the equivalent smaller regions.

The previous plots indicates that for the geometrical configuration with cilia inclined in the direction of magnetic field rotation, it is possible to attain a global net fluid motion in the direction of the magnet, thus indicating a micro-pump type application for such a condition. To a slightly lesser extent, this is also attained in the radial mounting of cilia. On the other hand, the cilia inclined counter rotation does not allow any global fluid motion, thus suggesting a micro-mixer application for such a geometrical configuration.

However, this conclusion must be confirmed by the results on turbulent kinetic energy, *i.e.* on *rms* fluctuations induced by locally generated turbulence which help increasing the amount of mixing. This quantity appears to be a good parameter to describe the effect of such rigid cilia motion (except at the root) in addition to those derived from the mean field. To this end, the square root of the sum of squared standard deviations of tangential and radial velocity components has been computed and is shown in Figure 13 for the three geometrical configurations of the cilia. Assuming a planar flow, which is reasonable due to the small height of the gap, this quantity is just proportional to the turbulent kinetic energy. It is confirmed that in the geometrical configuration with cilia mounted in the direction of the rotating magnet, the fluctuations are rather small (maximum value around 4 mm/s), and all the momentum transferred from cilia to the fluid is used for attaining a net flow. On the other hand, for the cilia mounted in the radial position, there are large values of turbulent kinetic energy (maximum value higher than 7 mm/s), thus allowing a more useful mixing for this geometrical configuration. It is important to point out again that this configuration is also the one ensuring a net flow, even if less than in the previous case. Lastly, the geometry with cilia mounted counter rotation, even if ensuring quite large values of turbulent kinetic energy, similar to those of the radial mounting, do not seem to attain a homogeneous distribution of fluctuations all over the field, rather being concentrated at the vortex center due to its oscillations.

4. Conclusions

In the present investigations, three main configurations of cilia are considered in order to determine which is the most suitable to be employed as a micro-pump or a micro-mixer. In order to perform experiments as reliable as possible, a scale up laboratory simulation is performed by keeping the Reynolds number as small as in real conditions.

The main result of the study is that with a simple change in geometrical inclination of the cilia (which are mostly rigid, except at the root), it is possible to attain different behaviors to be used in practical applications. The reason for this resides into the interaction among the alternate motion of cilia along their length and the surrounding fluid. In the case of cilia inclined in the rotation direction and partially in the case of pure radial configuration, their backward motion does not balance the forward one expecially close to the cilia root. On the other hand, the situation is almost symmetric among forward and backward motion for the case of cilia in counter-rotation position.

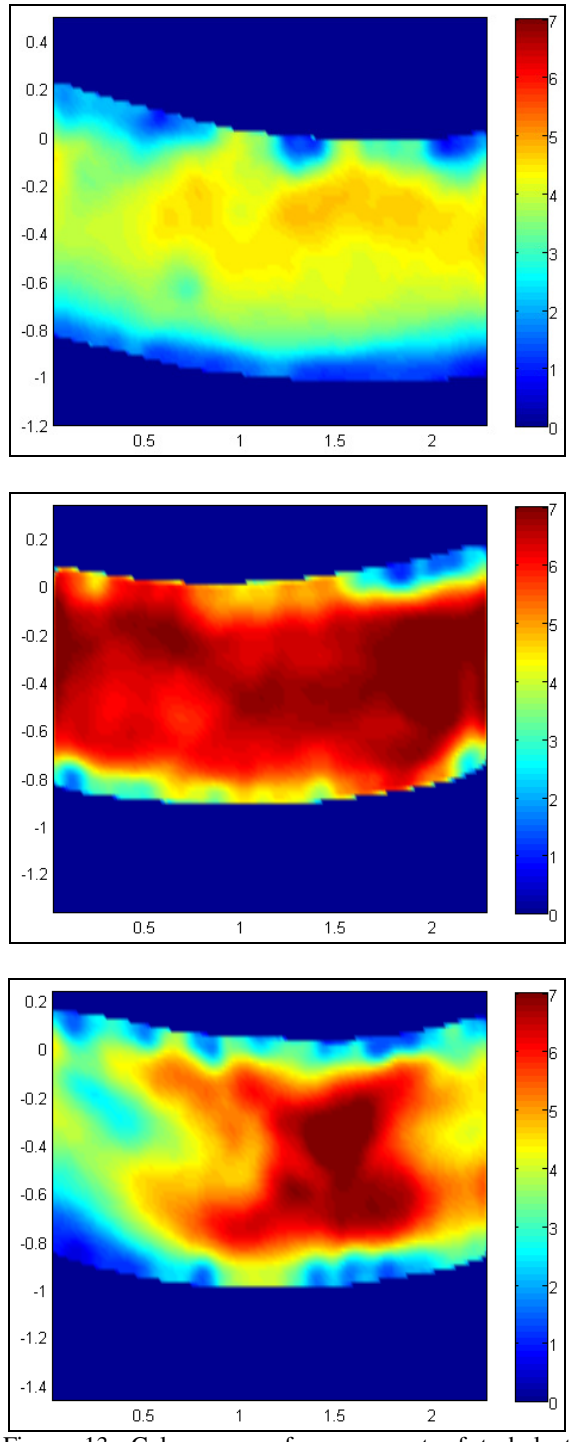

Figure 13. Color maps of square root of turbulent kinetic energy for the cilia inclined in the direction of rotation (at the top), in radial position (at the middle) and counter rotation (at the bottom). The axis are made non-dimensional by the cavity radius (1 cm), whereas the colobar is in mm/s.

References

Hussong J, Schorr N, Belardi J, Prucker O, Ruhe J, Westerweel J (2011a). Experimental investigation of the flow induced by artificial cilia. *Lab Chip*, 11(12): 2017-2022.

Hussong J, Breugem WP, Westerweel J (2011b). A continuum model for flow induced by metachronal coordination between beating cilia. *J. Fluid Mech*, 684: 137-162.

Kallio P, Kuncova J (2004) Microfluidics. *Technology Review*, 158.

Khaderi SN, Craus CB, Hussong J, Schorr N, Belardi J, Westerweel J, Prucker O, Rühe J, den Toonder JMJ, Onck PR (2011). Magnetically-actuated artificial cilia for microfluidic propulsion. *Lab Chip*, 11: 2002-2010.

Laser DJ, Santiago JG (2004). A review of micropumps. *Journal of micromechanics and microengineering* , 14: R35–R64.

Lindken R, Rossi M, Grosse S, Westerweel J (2009). Micro-particle image velocimetry PIV: Recent developments, applications, and guidelines. *Lab Chip*, 9(17): 2551-2567.

Niedermayer T, Eckhardt B, Lenz P (2008). Synchronization, phase locking, and metachronal wave formation in ciliary chains. *Chaos*, 18: 037128.

Purcell EM (1977). Life at Low Reynolds Number, *American Journal of Physics*, 45(1): 3-11.

Santiago JG, Wereley ST, Meinhart CD, Beebe DJ, Adrian RJ (1998). A particle image velocimetry system for micro fluidics. *Exp. Fluids*, 25(4): 316-319.

Squires TM, Quake SR (2005). Microfluidics: fluid physics at the nanoliter scale. *Reviews of modern physics*, 77: 977-1026.

Vogel S (1996). *Life in Moving Fluids: The Physical Biology of Flow*. Princeton University Press, Princeton.